

Research Article

Development of Dual Power Multirotor System

Chin E. Lin and Thanakorn Supsukbaworn

Department of Aeronautics and Astronautics, National Cheng Kung University, Tainan 701, Taiwan

Correspondence should be addressed to Thanakorn Supsukbaworn; ming6842@hotmail.com

Received 20 February 2017; Revised 13 April 2017; Accepted 30 April 2017; Published 30 July 2017

Academic Editor: Paolo Tortora

Copyright © 2017 Chin E. Lin and Thanakorn Supsukbaworn. This is an open access article distributed under the Creative Commons Attribution License, which permits unrestricted use, distribution, and reproduction in any medium, provided the original work is properly cited.

Vertical take-off and landing (VTOL) aircraft has good flight characteristics and system performance without runway. The multirotor system has been tried to expand into larger size for longer endurance or higher payload. But the motor power to endurance ratio has been limited. Due to the specific energy of gasoline being much higher than battery, introducing gasoline engine into multirotor system can be considered. This paper proposes a dual power multirotor system to combine a quadrotor using gasoline engines to provide major lift in shorter arm with another quadrotor using brushless DC motors to offer most controllable force with longer arm. System design, fabrication, and verification of the proposed dual power multirotor system development are presented. Preliminary flights have achieved 16 kg payload for long endurance flight. This is useful for various applications with advanced improvements.

1. Introduction

The struggle to improve flight endurance and flight performance of multirotor has made efforts for decades. From the beginning of the past decade, the multirotor development has accomplished relatively small size for experimental use. It then becomes popular for its usefulness in aerial photography and other related applications that lead to requirement in payload and flight time [1]. Multirotors have now been popular in every aspect from flying toy to professional use. However, with the limitation of battery technology [2, 3], the flight endurance has not been improved much in the past decade. How to improve the payload and flight endurance can be a significant job to deal with. This paper presents the new type of multirotor using dual power sources from gasoline engine and electric brushless DC (BLDC) motor. The design goal tries to extend the limitation of the electric multirotor while still conserving its advantage.

Flight stabilization of multirotors has been currently achieved by fast and accurate response of BLDC motor with the advanced technology of miniature MEMS sensor in the past years. The MEMS sensors allow the mass production with lower cost and also reduce the size of the overall system [4]. The MEMS sensors are not only more efficient, accurate,

and flexible compared to the piezoresistive type gyroscope [5] or even more advanced compared in mechanics but also very economical to laser-ring gyroscope. Although MEMS sensors have lots of advantages, there are some drawbacks by characteristics. The offset drifting of reading value and scaling error are affected by changing environment and state of the sensors. It is also more sensitive to vibration and noise in the system than other systems [6].

The sensorless BLDC motor control enables the efficient and accurate brushless motor control system with smaller size [7]. Brushless motor has a lot of advantages compared to brushed motor because of no commutator brush. The brush of brushed motor will wear out after some period of time and might lead to failure of control system. BLDC has longer lifetime and higher power output at the same size when compared to a brushed motor. Active freewheeling [8] and regenerative braking make BLDC motor controller even more efficient and precise in control [9].

Multirotor has advantage due to its simplicity, stability, flexibility, low cost, and being simple in manufacturing and maintenance. Mechanical simplicity is the major advantage over helicopter. The maneuverability and flexibility are the major advantage compared to fixed wing aircraft. However, its efficiency is far less than fixed wing

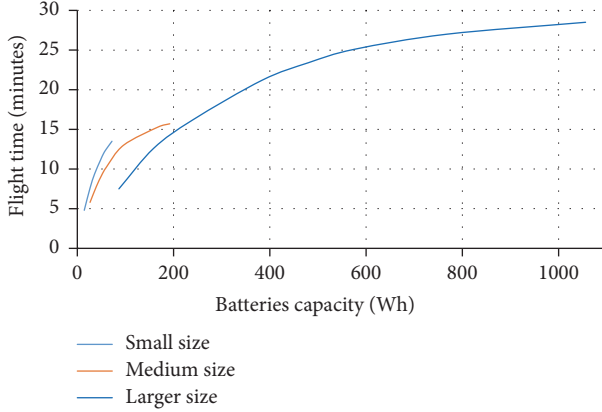


FIGURE 1: Performance of battery capacity to flight time.

aircraft and less than helicopter when compared at the same size. This is because the effective Reynolds Number at the lift generation plane of multirotor is much higher than helicopter and fixed wing aircraft. While helicopter also has rotating blades serving as primary lifting plane, it has less disc loading than multirotor and less influential flow from multiple rotors to result in higher efficiency [10, 11].

The design concept of the proposed multirotor system preserves the simplicity of multirotor while increasing its payload and flight time performance. The causes of endurance problem of the traditional multirotors mainly result from the fact that the energy density of battery at present is not high enough to supply this type of helicopter for higher endurance. Several designs tried to extend quadrotor into hexarotor or octorotor for increasing weight capability. Increasing endurance requires heavier battery. This in turn leads to a heavier aircraft where after some point the effectiveness of this solution is too low [12]. Motor lift and battery become performance saturated in weight balancing with little overall contribution as shown in Figure 1 from the eCalc simulation report [13]. The simulation data is based from the average economical setup available currently. The setting is done through eCalc simulation. The only variable for the same setup is the battery size which is proportional to battery weight. Each estimated flight time is plotted to the figure to show the relation between battery size and estimated flight time. The maximum battery size of each setup is closely related to the required hovering power for each motor to reach 80%.

From Figure 1, the small size configuration shows that the flight time increases before the limitation of its size. The size is then increased to medium size and larger size with significant difference. As the battery size increases, the energy capacity as well as its weight is increased. However, as the capacity increases, the effectiveness of battery capacity to flight time improvement is reduced. The analysis data for Figure 1 can be found in Tables 3, 4, 5, and 6.

There are many attempted methods to solve this inadequate endurance and payload problem. One of the popular solutions is to have many multirotor systems to operate as a swarm [14]. Although this might increase the coverage range

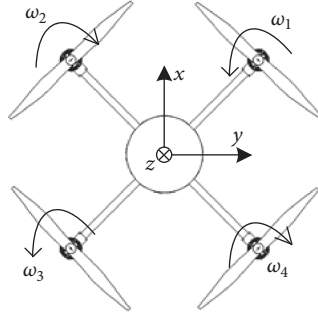


FIGURE 2: Quadrotor axis and actuator definition.

of operation, it reduces the flexibility of application due to the fact of more equipment as the swarm size increases. This does not solve the problem of one single heavier payload for longer endurance. Some methods also include landing platforms being placed along mission area. This method may induce the complexity of automatic take-off and landing along the mission area. If the mission is to be autonomous, the advanced facility and the multirotor itself also have to be equipped with more supporting devices to support the scenario.

There are also hybrid designs in power propulsion system in order to change the gasoline engine power to electric or vice versa [15]. Gasoline has higher specific energy of 46.4 MJ/kg compared to battery of 0.36~0.95 MJ/kg [16, 17]. It is quite favorable to adopt gasoline engine for the VTOL system. However, such method could lead to extra weight or complication in the system which leads to less reliability in system performance [18]. The preliminary study shows that the gasoline engine could be stabilized under favorable condition for multirotor [19]. Therefore, the idea of creating dual power system but preserving the simplicity of multirotor aircraft is introduced in this paper. The main idea is to magnify the advantage of each system to cover the drawback of the other.

2. Dual Power Multirotor Design Concept

2.1. Mechanical Design. Quadcopter is a type of multirotor, as shown in Figure 2. Its movement and control are driven by controlling ω_1 , ω_2 , ω_3 , and ω_4 . Differentiating BLDC motor speed on diagonal axes generates different torque to result in controllable angular moment around z -axis of the aircraft. Differentiating motor speed between each side generate moment for x -axis and y -axis which tilt the aircraft. Considering the quadcopter, a symmetric structure is assumed with four arms aligned with axis rotated 45 degrees by z -axis.

Thus, the inertia is diagonal matrix I , where $I_{xx} = I_{yy}$:

$$I = \begin{bmatrix} I_{xx} & 0 & 0 \\ 0 & I_{yy} & 0 \\ 0 & 0 & I_{zz} \end{bmatrix}. \quad (1)$$

The rotation rate of propeller, which is denoted as ω_i in Figure 1, creates force in the propeller axis. The angular velocity and acceleration of the rotor create torque τ_{M_i} around the rotor axis [20].

$$\begin{aligned} f_i &= k\omega_i^2, \\ \tau_{M_i} &= a\omega_i^2 + I_M\dot{\omega}_i, \end{aligned} \quad (2)$$

where the lift constant is k , the drag constant is a , and the inertia moment of the rotor is I_M . In general case, the effect of $\dot{\omega}_i$ is considered to be small so that it is omitted. Note that (2) assumes that the relation of force and torque is proportional to square of propeller rotation speed. In actual case, it depends on the blade profile of propeller which may have different variation.

$$T = \sum_{i=1}^4 f_i = k \sum_{i=1}^4 \omega_i^2. \quad (3)$$

The rotor forces create thrust T in the direction of negative body z -axis. Torque τ_B consists of the torques τ_x , τ_y , and τ_z in the direction of corresponding angle.

$$\tau_B = \begin{bmatrix} \tau_x \\ \tau_y \\ \tau_z \end{bmatrix} = \begin{bmatrix} lk(\omega_2^2 + \omega_3^2 - \omega_1^2 - \omega_4^2) \cos(45^\circ) \\ lk(\omega_1^2 + \omega_2^2 - \omega_3^2 - \omega_4^2) \cos(45^\circ) \\ \sum_{i=1}^4 \tau_{M_i} \end{bmatrix}, \quad (4)$$

where l is the distance between rotor and the center of mass of the quadcopter. The roll movement is acquired by increasing 2nd and 3rd rotors velocity and reducing 1st and 4th rotors velocity. In a similar way, the pitch movement is generated by increasing 1st and 2nd rotors velocity and decreasing 3rd and 4th rotors velocity. The yaw movement is generated by increasing the 2nd and 4th rotors velocity while decreasing velocity of 1st and 3rd rotors. The control power of x -axis and y -axis is influenced by the arm length l and the thrust force produced from the motor to result in $k\omega_i^2$. Thus, extending the arm length l of the motor support beam increases the control effectiveness of the motor. Structural strength has to be considered while extending the beam outward.

From the above equations, to suppress the control power is to reduce the length between the rotor and center of gravity l while increasing power is doing reversely. Also, considering the two systems which have different parameter a , k , and I_M , since it is necessary to account for all the effect of the torque in roll, pitch, and yaw axis by necessary counter force, the proposed idea is to design two systems that have their own equilibrium state of zero moment around axes. The less stabilized system is placed in the inner circle where it has less control power by reducing its arm length l . In contrast, the control power of the reliable part system increases its arm length outward for better performance.

The design concept builds a gasoline engine powered quadrotor on a BLDC motor powered quadrotor. It is termed

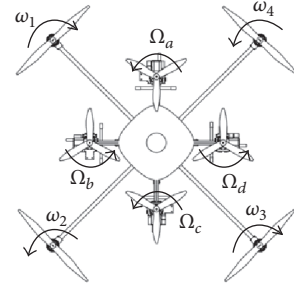


FIGURE 3: The proposed QiQ multirotor configuration.

as quadrotor in quadrotor, QiQ. The system design introduces the gasoline engines to supply the major lifting power while letting the electric motor handle the control stabilization, such that it is favorable for stabilization to increase the motor control effectiveness by reducing the effect of gasoline engine uncertainty to stability of aircraft. As discussed above, the control effectiveness of each motor or engine varies by distance of the unit to center of gravity of the aircraft. The reasonable configuration for this requirement is to move gasoline engine closer to center of gravity and extend the electric motor outward. The preliminary configuration of the proposed QiQ multirotor system is shown in Figure 3.

Two pairs of engine have each pair of rotation on opposite direction to generate counter torque as they spin the propellers. The pair of CW rotating engine counter the torque from CCW rotating engine and vice versa. This idea is better than other alternative ideas such as tilting the engines or motors in order to compensate the force because the engines contribute lift force vector purely pushing upward vertically only. The power of engines can efficiently be used for lifting force alone. In addition, the byproduct torque generated from the propeller is cancelled by the opposite side propeller without any extra mechanism. This design is also optimized to utilize the lifting plane available to the maximum by placing the lift from the engine at the space between motor arms.

Considering (4) for the inner quadrotor frame resultant force and moment output,

$$\tau_{B_{in}} = \begin{bmatrix} l_{in} k_{in} (\Omega_b^2 - \Omega_d^2) \\ l_{in} k_{in} (\Omega_a^2 - \Omega_c^2) \\ \sum_{i=1}^4 \tau_{M_i} \end{bmatrix}, \quad (5)$$

$$T_{in} = \sum_{i=1}^4 f_{ini} = k_{in} \sum_{i=a}^d \Omega_i^2,$$

$$\tau_{M_{in,i}} = a_{in} \Omega_i^2.$$

The propeller velocity of the internal frame is assumed to have the same speed $\Omega_1 = \Omega_2 = \Omega_3 = \Omega_4$. The airframe is also

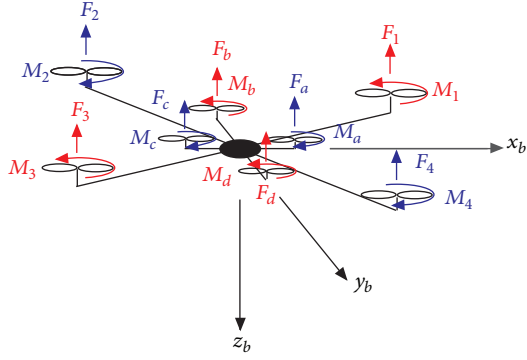


FIGURE 4: Rotor force and torque distribution analysis.

assumed in nearly static condition, where there is no sudden change to the frame attitude. This results in

$$\tau_{Bin} = \begin{bmatrix} 0 \\ 0 \\ 0 \end{bmatrix}, \quad (6)$$

$$T_{in} = 4 \times k_{in} \Omega^2.$$

Equation (6) shows the additional central frame to purely contribute lift force and result in zero moment output if all engines RPM are well controlled. The QiQ dynamics or equation of motion can be constructed by transformation of body frame motion to earth frame. In the body axis, the rotor force and torque distribution on its frame are illustrated in Figure 4. The equation of motion can be formulated as follows.

Under steady state,

$$\dot{z} = \dot{\phi} = \dot{\theta} = \dot{\psi} = \dot{w} = \dot{p} = \dot{q} = \dot{r} = 0, \quad (7)$$

$$w = p = q = r = 0.$$

Then the equation of motion can be constructed by

$$\begin{bmatrix} \dot{x} \\ \dot{y} \\ \dot{z} \end{bmatrix} = \begin{bmatrix} C_\theta C_\psi & -C_\phi S_\psi + S_\phi S_\theta C_\psi & S_\phi S_\psi + C_\phi S_\theta C_\psi \\ C_\theta S_\psi & C_\phi C_\psi + S_\phi S_\theta S_\psi & -S_\phi C_\psi + C_\phi S_\theta S_\psi \\ -S_\theta & S_\phi C_\theta & C_\phi C_\theta \end{bmatrix} \begin{bmatrix} u \\ v \\ w \end{bmatrix},$$

$$\begin{bmatrix} \dot{\phi} \\ \dot{\theta} \\ \dot{\psi} \end{bmatrix} = \begin{bmatrix} 1 & S_\phi t\theta & C_\phi T_\theta \\ 0 & C_\phi & -S_\phi \\ 0 & S_\phi & C_\phi \end{bmatrix} \begin{bmatrix} p \\ q \\ r \end{bmatrix},$$

$$\begin{bmatrix} \dot{u} \\ \dot{v} \\ \dot{w} \end{bmatrix} = \begin{bmatrix} -qw + rv \\ pw - ru \\ -pv + qu \end{bmatrix} + \begin{bmatrix} -W \sin \theta \\ W \sin \phi \cos \theta \\ W \cos \phi \cos \theta \end{bmatrix} + \frac{1}{m} \begin{bmatrix} 0 \\ 0 \\ F_z \end{bmatrix},$$

$$\begin{bmatrix} \dot{p} \\ \dot{q} \\ \dot{r} \end{bmatrix} = \begin{bmatrix} I_{xx} & 0 & I_{xz} \\ 0 & I_{yy} & 0 \\ I_{xz} & 0 & I_{zz} \end{bmatrix}^{-1} \begin{bmatrix} 0 & r & -q \\ -r & 0 & p \\ q & -p & 0 \end{bmatrix} \begin{bmatrix} I_{xx} & 0 & I_{xz} \\ 0 & I_{yy} & 0 \\ I_{xz} & 0 & I_{zz} \end{bmatrix} \begin{bmatrix} p \\ q \\ r \end{bmatrix}$$

$$+ \begin{bmatrix} I_{xx} & 0 & I_{xz} \\ 0 & I_{yy} & 0 \\ I_{xz} & 0 & I_{zz} \end{bmatrix}^{-1} \begin{bmatrix} M_x \\ M_y \\ M_z \end{bmatrix}, \quad (8)$$

where ϕ , θ , and ψ are roll, pitch, and yaw angle, respectively. u , v , and w are linear acceleration components of the body frame. p , q , and r are angular velocity components of the body frame.

The equation of motion is transformed into

$$\dot{x} = \cos \theta \cos \psi u \quad (9a)$$

$$+ (-\cos \phi \sin \psi + \sin \phi \sin \theta \cos \psi) v,$$

$$\dot{y} = \cos \theta \sin \psi u \quad (9b)$$

$$+ (\cos \phi \cos \psi + \sin \phi \sin \theta \sin \psi) v,$$

$$m\ddot{x} = F_z (\sin \phi \sin \psi + \cos \phi \sin \theta \cos \psi), \quad (10a)$$

$$m\ddot{y} = F_z (-\sin \phi \cos \psi + \cos \phi \sin \theta \sin \psi), \quad (10b)$$

$$m\ddot{z} = W + F_z \cos \phi \cos \theta. \quad (10c)$$

The attitude control in the body frame is represented by the following equations:

$$M_x = (F_b \ell_1 - F_d \ell_1) + \frac{\ell_2}{\sqrt{2}} (F_1 + F_2 - F_3 - F_4), \quad (11a)$$

$$M_y = (F_a \ell_1 - F_c \ell_1) + \frac{\ell_2}{\sqrt{2}} (F_1 - F_2 - F_3 + F_4), \quad (11b)$$

$$M_z = (M_a - M_b + M_c - M_d) - M_1 + M_2 - M_3 + M_4, \quad (11c)$$

where m is the mass of the system. x , y , and z are translation components in the body frame F_a , F_b , F_c , F_d . M_a , M_b , M_c , M_d are engine thrust and torque, respectively. $\ell_1 = \ell_2 = \ell_3 = \ell_4$ is the length of moment arm of electrical motor from center of gravity where $\ell_1 = \ell_2 = \ell_3 = \ell_4$ in our design and $\ell_a = \ell_b = \ell_c = \ell_d$ represents the length of moment arm of engine to center of gravity. The total thrust force can be calculated by the following equation:

$$F_z = -(F_a + F_b + F_c + F_d + F_1 + F_2 + F_3 + F_4). \quad (12)$$

The size of gasoline engine has been developed smaller to increase its capability and reliability over past decade. Its capacitor discharge ignition (CDI) units allow accurate



FIGURE 5: Aluminum central plate structure.

ignition timing and get easier to startup especially at cold start [21]. The hall sensor installed on engine shaft also provides a good source for RPM sensing for engine speed controller. This has advantages over Nitro type small engine, where the combustion cycle is not controlled timely by ignition system.

However, the gasoline still has its complexity. There are two to three needles for fuel-air mixture adjustment. For system setup, the O.S. GT-33 engine is selected [<http://www.osengines.com/engines-airplane/osmgl533/index.html>]. It has two mixture needles: one to control fuel flow at low-to-medium speed and hold constant through the rest of the region and the other to control the fuel flow rate at high engine speed. They are called low-speed needle and high-speed needle, respectively. By carefully adjusting both needles, the engine characteristics, performance, and stability can appropriately be controlled. However, due to any difference of engines caused from setup or manufacturing, each engine has different best needle setup for itself. This makes slight difference in engine characteristics. This engine difference is considered as a system uncertainty.

Engine has one big disadvantage over electric motor for its serious vibration during operation. Vibration is dangerous to this system for structure and flight stabilization. In the QiQ design, there are four engines that run at the same time. The best way to handle this problem is to isolate the engine vibration from other parts of the structure. There are many types of the shock absorber available. They are molded elastomer mount, spring damper, air isolator, wire rope isolator, and so forth. In the QiQ developing phase, the wire rope isolator is found by experiments as the most suitable type of isolator. The wire rope isolator accepts high traction axial load, which is thrust force for the QiQ. Gasoline does not corrode the metal like it does to rubber or other kinds of hydrocarbon materials. It is also commercially available and customizable at reasonable cost. Experiment later shows more evidence about necessity of this shock absorber to multirotor stabilization.

To enforce the overall structure, two identical aluminum plates are designed and fabricated as the central structure, as shown in Figure 5. The plates are machined with appropriate slots and holes to sandwich and fix structural beams for engine and motors. Four big cutouts and holes in the center of the aluminum plate as shown in Figure 5 are for wiring and weight reduction. The plate has thickness of 4 mm. BLDC motor support arm is made of carbon fiber and has thickness

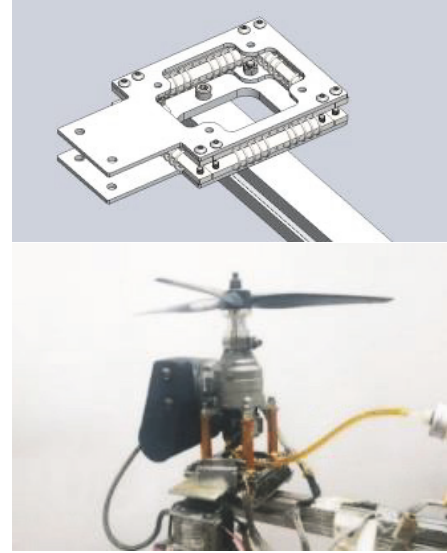


FIGURE 6: Wire type shock absorber and installation.



FIGURE 7: The preliminary flight test of QiQ using plastic fuel tank.

of 3.5 mm, with outer diameter of 25 mm and length of 90 cm. The motor support arms are connected to central plate through fixing clamp with 10 cm offset from the center to result in 100 cm distance from motor to center.

GT-33 engines are mounted on the end of the shorter angle aluminum beam which is fixed on the central aluminum plate. Wire type shock absorber is used to reduce the engine vibration, as shown in Figure 6. Servo motors are installed at the end of the long arm extending from the aluminum plate. The ignition controller unit and its battery are installed beneath the top central aluminum plates, while the servo is installed next to the ignition controller units. This separation allows vibration isolation from engine to the main frame but maintains servo to have the same reference frame with engine. The engine support angle aluminum beam dimension is 30 × 30 mm cross section and is 45 cm in length. Engine propeller center has distance of 50 cm from frame center.

Plastic fuel tank is used in the prototype QiQ airframe for gasoline. The tube is set as pointing downward for refueling with a fuel filter at the end of the longer tube inside the fuel tank, as shown in Figure 7. The filter's weight pushes the tube end down into the fuel. The cap is sealed but has a breathing

TABLE 1: Engine fuel consumption.

RPM	5500	6300	7200
Consumption (cc/hr/engine)	540	720	1074

hole to equalize the inside air pressure to ambient pressure. The GT-33 engine does not require the exhaust pressure back to increase pressure inside the fuel tank.

The gasoline engine uses Master Airscrew 16 × 10 3-blade propeller. The electric stabilization part KDE5215XF-435 BLDC motor is selected from KDE Direct [https://www.kde-direct.com/products/kde5215xf-435] using Multistar 18" × 6.1" double-blade wood propeller [https://www.hobbyking.com/hobbyking/store/_58197_Multistar_Timber_T_Style_Propeller_18x6_1_White_CW_CCW_2pcs_.html]. The propeller is designed for big multirotor. It has less pitch compared with normal airplane propeller, thus producing less drag, but has disadvantage of being less capable for forward flight.

2.2. Flight Characteristics Design. In order to achieve the maximum flight performance on each design scenario, the energy matching between gasoline and electric batteries has to be matched for both gas/electric system capability to use all the carried fuel and batteries in flight. The fuel consumption of engines at optimum condition is examined. These data are taken from the 4 averaged different engines which are adjusted to their optimum conditions. The tests were done in a 27°C calm day at 5 m elevation over sea level. The oil-fuel ratio was 3.75%. The Master Airscrew 16 × 10 3-blade propeller is used in this experiment [https://www.masterairscrew.com/products/3-blade-16x10-propeller]. The preliminary experiment is shown in Table 1 and Figure 6.

The engine performance and characteristics are studied by the test platform shown in Figure 8. The engine (1) is placed on top of the strain gauge (4) with the throttle servo (2) and CDI unit (3). The CDI unit power is supplied by the battery (9). The CDI hall sensor output is connected to both CDI unit and the microcontroller (7). Fuel tank (5) is placed next to the strain gauge as the fuel supply for engine. The strain gauge is connected with bridge circuit and signal conditioner (6). The RPM and thrust signal are then connected to microcontroller and transferred to laptop computer (8) for analysis.

The test result shows that the thrust force output from GT-33 engine with Master Airscrew 16 × 10 3-blade produces considered linear thrust to engine speed changes, as shown in Figure 9. So the engine input from control system should be noted in terms of RPM.

In a similar manner, the electric motor power consumption is also examined by the test platform as shown in Figure 10. The motor (2) and propeller (1) are placed on top of the strain gauge (3). The strain gauge signal is passed through bridge circuit and signal conditioner (4) and then connected to microcontroller (10). The data from microcontroller is captured with laptop computer (7) for analysis. The current and voltage of system are measured by hall sensor watt meter

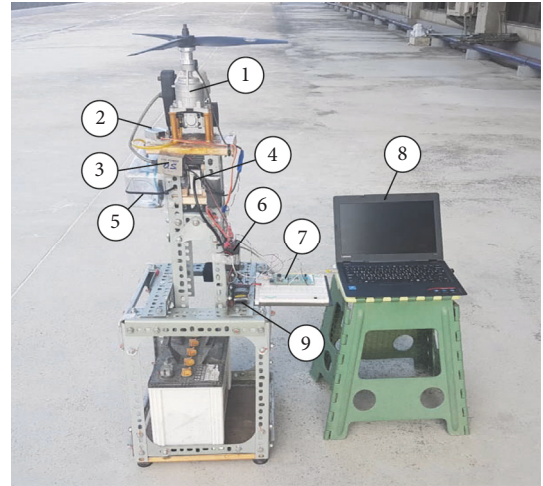


FIGURE 8: Engine thrust and RPM test platform.

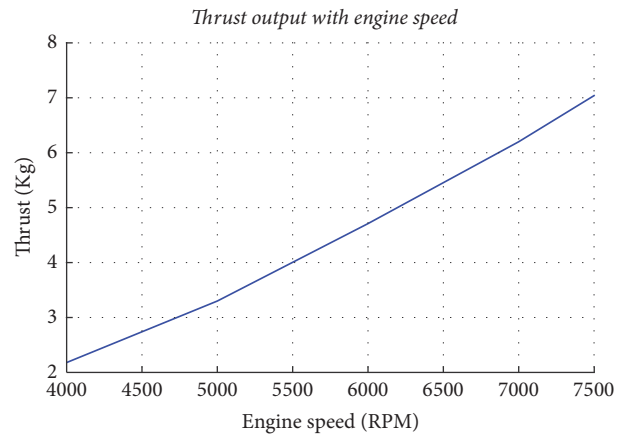


FIGURE 9: Engine thrust output versus engine speed.

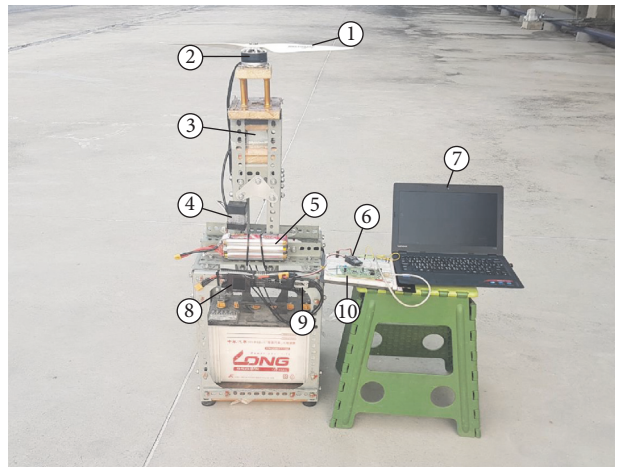


FIGURE 10: Electric motor thrust test platform.

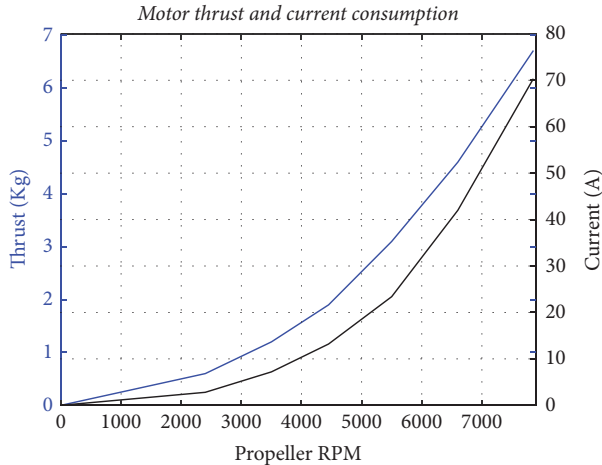


FIGURE 11: Electric motor thrust output and current versus motor speed.

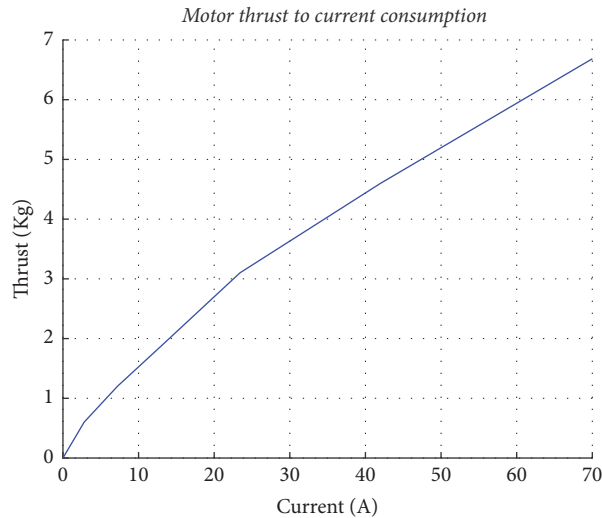


FIGURE 12: Electric motor thrust output versus current.

(8). The radio receiver (6) is controlled to electronic speed controller (9) to control the motor. The BLDC motor in the experiment uses KDE Direct 5215XF-435KV running at 22.2 V nominal voltage, using Multistar 18 × 6.1 propeller. The characteristics data from preliminary flight test are shown in Figure 11.

From Figure 12, the RPM and thrust for KDE Direct 5215XF-435KV BLDC motor with Multistar 18 × 6.1 propeller are not linear. However, since the electronic speed controller uses input as power consumption which is varying with current, the current consumption and thrust are not linear at very low current but rather linear when the current consumption is higher than 10 A, as shown in Figure 12. The rest of throttle level can be considered as linear for control system simplification.

The QiQ design has its target to the longest endurance at one hour. QiQ is also designed as adaptable for high payload application too. After fabrication of the first prototype, the total empty weight without fuel and main batteries is

TABLE 2: Various flight configurations.

Flight condition	Maximized endurance	Balanced	Maximized payload
Empty weight	19.6 kg	19.6	19.6
Fuel load	3.2 kg	1.6	1
Battery weight	12.8 kg	12.8	12.8
Payload	0 kg	12	20
Total weight	36 kg	46.4	53.8
Engine thrust	24 kg	28	29
Motor thrust	12 kg	18.4	24.8
Endurance	60 min	28	20

19.6 kg. The battery unit are four of 6 cell lithium polymer, 5200 mAh capacity battery, each weight 820 grams. From the preliminary test, the maximum engine thrust can be 7.02 kg, and the BLDC motor thrust can vary from 2 kg to 6 kg at hovering condition. The maximum lifting force from both quadrotor systems can provide 66 kg maximum lift. While the maximum power is huge when compared to the empty weight of 19.6 kg, the force of motor comes associated with current consumption and affects flight time. There are several flight configurations of QiQ being proposed for reference as in Table 2.

2.3. Engine Controller Design. The stabilization of multirotor requires fast RPM response from the stabilization motor. Individual stability from all units providing lift to the system may affect the overall flight stability and quality of the QiQ multirotor system. Although BLDC motor provides fast response to the given input, the gasoline engine does not act in the similar response. The gasoline engine power output is usually controlled by air inlet value which controls the quantity of fuel and air which goes into the combustion chamber. Carburetor acts as a mechanical controller for the engine. The performance and characteristics of the engine are adjusted by fuel-mixture needles. Just like any other air-breathing engine, gasoline engine is affected by environment such as atmosphere pressure, air temperature, and humidity. Engine temperature varying during runtime plays an important role to affect engine performance and characteristics. These are major challenges that would not allow open-loop control for engine RPM. The uncertainty from environment which affects engine might induce unwanted characteristics of engine, lead to instability flight, and affect flight performance dramatically.

Engine response in open loop has unpredictable characteristics. A preliminary study shows the response characteristics of engine and motors, as shown in Figure 13. From Figure 13, the engine response does not directly match with the throttle input. In contrast, it lacks stability in RPM sustenance. At the beginning, it cannot output the power in time but it follows the command but slowly with RPM increasing. It also cannot return to original RPM after the throttle is reduced. Conversely, the BLDC motor gives more precise and accurate response in speed control. The electronic speed controller (ESC) takes the desired power

TABLE 3: Simulation detail for each airframe configuration.

Simulation profile	Motor	Propeller profile	Propeller size	Frame weight (g)	ESC max current (A)	Battery C rating
Small	EMAX (MT1806 2280KV)	Master Airscrew Electric	4.7 × 3	250	30	45C/60C
Medium	EMAX (GT2215-10 1100KV)	Master Airscrew Electric	10 × 4	600	30	35C/50C
Large	EMAX (GT5325-09 325KV)	XOAR P/N Electric	28 × 4.7	1500	100	35C/50C

TABLE 4: Small-size quadrotor's configuration for flight time simulation and result.

Battery capacity (Wh)	Battery weight (g)	AUW (g)	Battery resistance (ohm)	ESC internal resistance (ohm)	Battery specific energy (MJ/Kg)	Flight time (min)
13.32	96	605	0.0108	0.008	0.4995	4.8
24.42	174	691	0.0059	0.008	0.5052	7.6
33.3	237	760	0.0043	0.008	0.5058	9.4
44.4	315	846	0.0033	0.008	0.5074	11.1
49.95	354	889	0.0029	0.008	0.5080	11.9
55.5	393	932	0.0026	0.008	0.5084	12.5
66.6	471	1017	0.0022	0.008	0.5090	13.5

TABLE 5: Medium-size quadrotor's configuration for flight time simulation and result.

Battery capacity (Wh)	Battery weight (g)	AUW (g)	Battery resistance (ohm)	ESC internal resistance (ohm)	Battery specific energy (MJ/Kg)	Flight time (minute)
24.42	174	1319	0.0066	0.008	0.5052	5.8
36.63	258	1412	0.0044	0.008	0.5111	7.8
46.62	330	1491	0.0035	0.008	0.5086	9.2
55.5	393	1560	0.0029	0.008	0.5084	10.2
88.8	627	1818	0.0018	0.008	0.5099	13
155.4	1095	2333	0.0012	0.008	0.5109	15.3
177.6	1251	2504	0.0011	0.008	0.5111	15.7

TABLE 6: Larger-size quadrotor's configuration for flight time simulation and result.

Battery capacity (Wh)	Battery weight (g)	AUW (g)	Battery resistance (ohm)	ESC internal resistance (ohm)	Battery specific energy (MJ/Kg)	Flight time (minute)
106.56	752	5407	0.0081	0.0025	0.5101	8.9
195.36	1376	6094	0.0044	0.0025	0.5111	13.8
296	2096	6886	0.0029	0.0025	0.5084	17.5
473.6	3344	8258	0.0018	0.0025	0.5099	21.5
592	4176	9174	0.0015	0.0025	0.5103	23
710.4	5008	10089	0.0012	0.0025	0.5107	24
947.2	6672	11919	0.0009	0.0025	0.5111	24.9
1302.4	9168	14665	0.0007	0.0025	0.5114	25

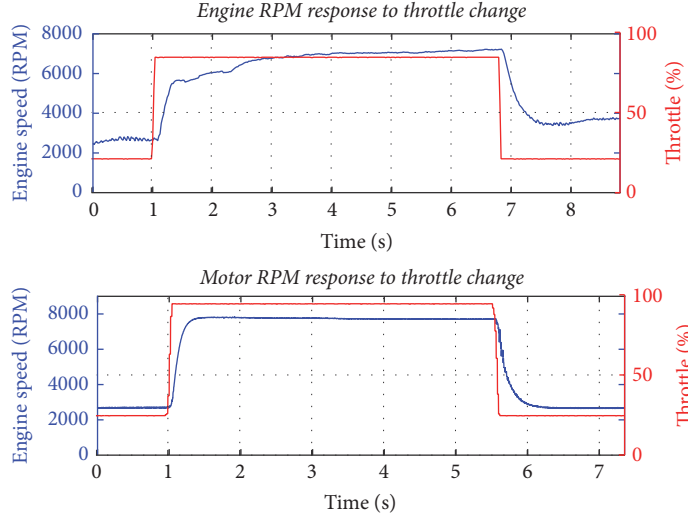


FIGURE 13: Step response comparison between gas engine and electrical motor.

output as the throttle input. The RPM is considered as an open-loop control in this case. Once the throttle is settled, the motor RPM will respond instantaneously and accurately. It also responds quickly when reducing the throttle back to its original position. Slowing down the motor speed takes more time in this test because the braking cannot be enabled. But this should be considerable enough for flight stabilization.

Engine linearity is another important issue in the engine RPM stabilization and its controller. The O.S. engine GT-33 carburetor data from manufacturer stated that 70–80% of maximum engine power develops within half of air inlet value. This serves as throttle input for the engine. From the preliminary experiment, the engine response to the throttle input is shown to be highly nonlinear. Before implementing PD controller, it is necessary to linearize the throttle input to reduce the complexity of introducing a PD controller. The incremental PD controller is then implemented to the system. These two combinations allow the system to respond to instant movement of RPM command as well as accurately tracking for servo optimum point.

In a mission starting from take-off to landing, engine controller has to change its mode in several times. There are three major modes required for the QiQ. (1) Startup mode is where the engine throttle is set to idle point of the engine. After that the engine can be started either by using electric starter or by slapping the propeller. (2) The second mode of the RPM controller mode activates the engine speed controller and will be activated through the whole flight. (3) For the final mode, the throttle cut-off mode can shut down the engine by reducing throttle to zero for several seconds until the engine is fully stopped.

In addition, the engine controller has to receive other commands or parameter settings from the flight controller or the ground station. Those parameters include controller gain, servo limit, and idle position. It is necessary to have data transfer mechanism to send modes,

parameters, and other commands from flight controller to the engine controller. Nevertheless, it is still necessary to keep a necessary bandwidth of RPM command stream from flight controller to engine controller. The RPM command is different from other kinds of data transfer because the command has to be synchronized with flight controller control loop. In addition, the RPM command data is streaming one-way from flight controller to engine controller.

One more thing to consider about communication between engine controller and flight controller is the reliability of the communication system. Engine itself generates a lot of EMI from its ignition system. Vibration from engine and other sources can affect the reliability of data transfer. Flight controller needs to ensure that the command it assigned is completely and correctly transferred to engine controller to keep machine state being tracked. The CAN Bus protocol meets all the requirements. CAN is a bus type of communication and two-way transmission with error-checking mechanism. Each message in CAN Bus required acknowledgment in transport layer [22].

If it appears that the message is not received by other nodes, the CAN Bus controller supports automatic retransmission. It is also proven in the automotive standard, where the scenario is similar to the QiQ design.

The CAN Bus serves as parameter and status report feedback from engine controller. This includes every message between flight controller and engine controller but not RPM command. The RPM command in CAN Bus is used instead of a dedicated wire for each engine controller. The RPM signal is Pulse Width Modulation (PWM) signal with frequency of 50 Hz.

Since control loop requires feedback signal from engines, it can theoretically and simply read from hall effect sensor installed on the shaft of the engine. The RPM sensor generates a pulse for each engine revolution. Engine controller then reads the pulse, calculates time difference between each pulse,

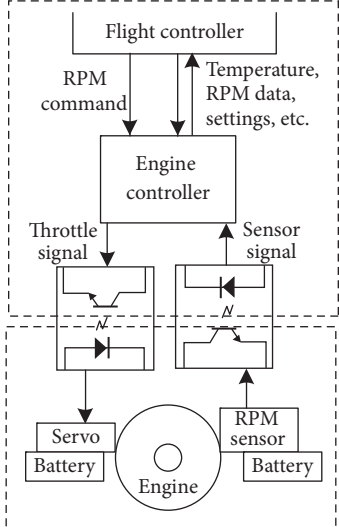


FIGURE 14: Engine controller diagram.

and gets the RPM data. However, in practice, the signal is severely disturbed by a very high frequency and very high amplitude noise. If the RPM sensor is connected directly to the main electronic system, it affects all of the signal input/output readings of the microcontroller. Moreover, the signal level output from the hall sensor is 0~1.5V, which is too low to trigger the MCU readings. The EMI noise also propagates through servo motor wires because they are necessary to be placed close to the engine.

To prevent the disruption of electronic system from EMI noise of engines, the isolation of electric system between noisy system and main system needs to be considered. The isolator needs to have a signal amplifier, where its robustness and simplicity are required. Its frequency response is better to be in the RPM signal than the high frequency noise range. In order to achieve the isolation, a transistor is introduced to amplify the RPM signal from the engine. The amplified signal drive TLP181 optoisolator is adopted to separate two power systems by the light transmission and light reception, as shown in Figure 14. Thus, the electrical noise in the line is isolated from the main electronic system. Moreover, the TLP181 has low speed frequency characteristic. This is favorable for us as we want to filter out the higher frequency unwanted signal. It is effectively absorbed by the optoisolator.

The servos also are found to be an EMI receptor to the power system after preliminary tests. Because it has to be installed close to the engine, the EMI from ignition can propagate through the air to the servo chassis. Although the EMI does not affect the servo itself, it induces a severe disturbance effect on the engine controller electronics. It is better to separate the power system of the servo as well. The optoisolator is used on the signal line from engine controller in a similar manner to RPM signal but without amplifier. It is shown in Figure 15.

Control loop of the engine controller is running at 50 Hz update rate, which matches the servo motor input frequency. The incremental PID controller is used in this design. The

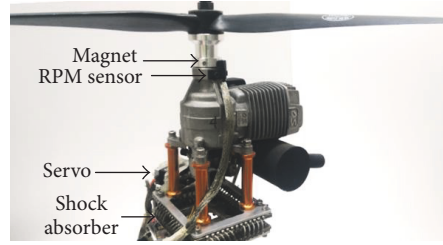


FIGURE 15: Engine sensor and shock absorber installation.

desired engine rotational speed (in RPM) is called setpoint. The difference between measured RPM and the setpoint is the error (E). The incremental PID controller's control algorithm is as follows:

$$U(k) = K_P E(k) + K_I \sum_{h=0}^k E(h) + K_D [E(k) - E(k-1)], \quad (13)$$

where k is the sampling number ($k = 0, 1, 2, \dots$), $U(k)$ is the output at k iteration, $E(k)$ is RPM errors at iteration k , and K_P , K_I , and K_D are proportional gain, integral gain, and derivative gain, respectively. According to the above formulations, $U(k-1)$ can be obtained from recursive method as follows:

$$U(k-1) = K_P E(k-1) + K_I \sum_{h=0}^{k-1} E(h) + K_D [E(k-1) - E(k-2)]. \quad (14)$$

Then, the incremental step can be obtained from subtraction of (13) and (14).

$$\Delta U(k) = K_P [E(k) - E(k-1)] + K_I E(k) + K_D [E(k) - 2E(k-1) + E(k-2)], \quad (15)$$

where $\Delta U(k)$ is the incremental output and it will be added to the last output $U(k)$ which is $U(k) = U(k-1) + \Delta U(k)$. This is the incremental PID algorithm used to control the QiQ. K_I is the key part of the engine controller as it allows the incremental controller to respond to error accordingly. K_P is required to respond to immediate error and fast change of setpoint. K_D is used for damping the oscillation and allows larger K_I for faster response without overshooting.

From the design of carburetor, the response of given input to the output RPM is not linear. PID controller is based on the linear system. Its parameter is not suitable for the whole range of operation. The engine response curve is steep at lower throttle and becomes less sensitive at higher throttle. The actuator linearization is adopted based on the captured data to normalize the response rate of the engine throughout the throttle range from 4000 RPM to 7500 RPM. Data is cut into two sessions for 4000~6000 RPM and 6000~7500 RPM to form two sections of linearization equation.

2.4. Flight Stabilization System. Attitude stabilization of multirotor is the key to make its fly. In fact, it is almost impossible to fly multirotor without the stabilization system. In the dual power QiQ case, more challenges lie on the higher inertia airframe. The smooth attitude response is required to make sure that engine and fuel will not be affected by the movements. The stabilization of the proposed design is based on those four outer electric motors. They act similar to a conventional quadrotor system. The difference of power in each motor generates moment that tilts the frame around its center of gravity. In the conventional electric multirotor, only motors and propellers are moving parts. However, in the dual power QiQ design, there is liquid gasoline with engines that are sensitive to quick movement. With too fast angular velocity of the body frame, the gasoline may splash to affect the center of gravity and form bubbles in the fuel. This will cause the engine to have unstable trembles due to the carburetor suction with air bubble from the fuel inlet. This may cause engine to get into intermittent instability or even shut down. Since these fast angular movements are caused by attitude stabilization controller in fast response, it is practical to set a limit over attitude response speed. Nevertheless, the accuracy and precision of the controller have to be preserved.

The flight control board uses STM32F427 as a main microcontroller in the proposed QiQ system [<http://www.st.com/en/microcontrollers/stm32f427-437.html>]. Flight controller obtains inertia data from InvenSense MPU-6500 [<https://www.invensense.com/products/motion-tracking/6-axis/mpu-6500>] which has 3-axis accelerometer and 3-axis gyroscope. The control board itself is also equipped with barometer but it is not used in this system. The sensor fusion algorithm runs at 4 kHz, which is high enough to give accurate attitude estimation even in case of fast movement or vibration.

The flight controller implements PD controller with PID inner loop to control roll and pitch angle, as shown in Figure 16. The key of inner loop PID controller is to react quickly at the lowest error to the angular rate of the QiQ. The integral part of PID controller compensates the external effect to stabilization. For example, if the installation of payload or airframe cannot satisfy the characteristics, the integral part will accumulate to offset the lifting force to keep the angular rate at desired level. The proportional and derivative parts are to respond to the immediate error which is required to have fast settling time.

The outer loop PD controller takes input from transmitter and outputs the desired angular rate. It has angular rate limiter to control the rate of response. In some cases, the angular rate should be slower, such as application with the onboard gimbal stabilization for onboard camera. The device may have poor response if the airframe rotates too fast. The proportional part of the outer PD describes how fast the control should respond to the error. Large proportional gain gives crisp response for the proposed QiQ system while slightly increasing its accuracy in overall. The derivative part prevents overshoot and controls system in smoothness.

For heading controller, the simple PID controller is used as in Figure 17. The controller only controls the rate of turning. The input is taken from transmitter. The more deflection

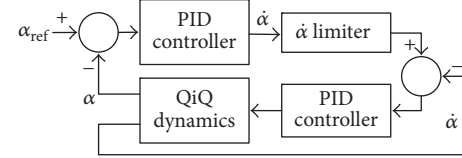


FIGURE 16: Roll and pitch PID stabilization controller diagram.

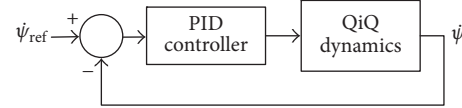


FIGURE 17: Yaw stabilization controller diagram.

the control stick applies, the faster heading changes. The integral part is the most important one in this controller because it allows the heading hold feeling to the pilot.

3. Implementation and Experiment Results

3.1. Shock Absorber Test Result. Shock vibration from reciprocating engine is not suitable for automatic stabilization system, especially when the accelerometer is used as a part of attitude estimation. Vibration also damages structure in long term by inducing fatigue, loosing fastener, disturbing other devices, and so forth. In the QiQ design, there are four engines running simultaneously such that the shock vibration of the engine should be minimized and prevent the vibration spreading.

Shock absorber performance is validated by comparison with the vibration of the test platform between two installation configurations. The configurations mount the engine with or without shock absorber. The MPU-6500 IMU is used to measure the acceleration of the frame. This IMU is similar to the one implemented on flight control. The acceleration limit of this accelerometer is ± 16 g. The result is shown in Figures 18 and 19.

The shock acceleration data are collected from the accelerometer in the axis of piston movement. It can be seen in Figure 18(a) that the sensor is saturated. The engine RPM is 7300 RPM at this condition. Figure 18(b) shows the snapshot of the measured acceleration. The oversaturation of the reading data is obvious. The actual acceleration is much higher than the sensor limit of 16 g. This saturation data could lead to large attitude estimation error of flight control system. It is also asymmetrical on both sides of acceleration due to compressing and expanding stage in each revolution of the two-stroke engine. It is also impossible to implement Inertial Navigation System (INS) related algorithm in the situation. The flight stabilization cannot be realized without resolving this problem.

After installing the engines on the shock absorber on the test platform, the vibration on the structure is dramatically reduced, as shown in Figure 19. Compared to the direct mounting data, the vibration acceleration is much over the limit of the accelerometer (16 g). The range of acceleration vibration readings from IMU is reduced to ± 5 g after using

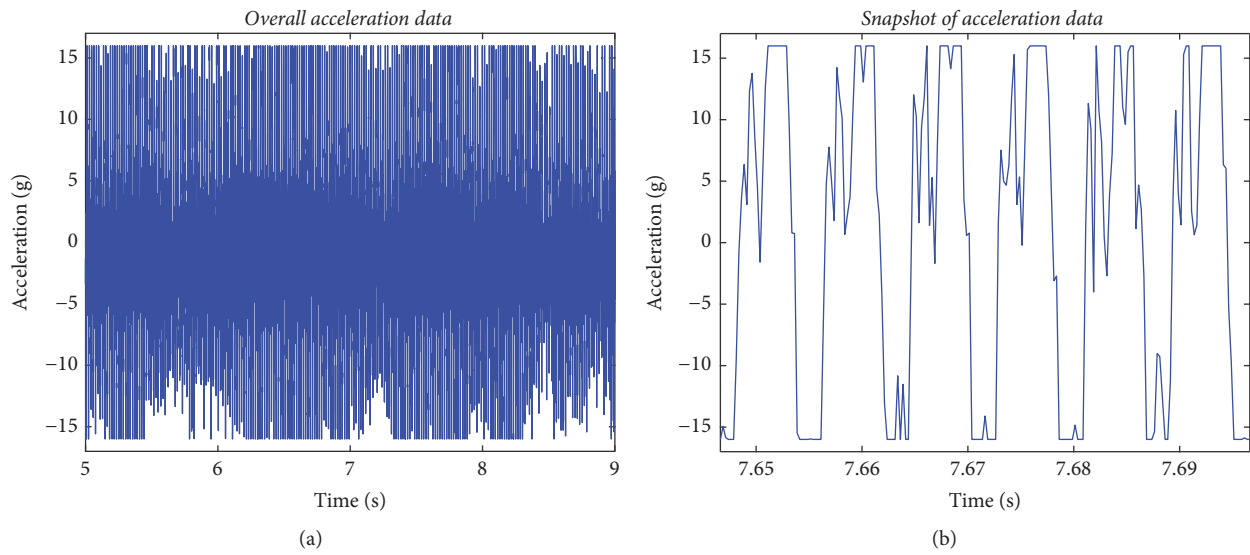


FIGURE 18: Measured acceleration data without shock absorber.

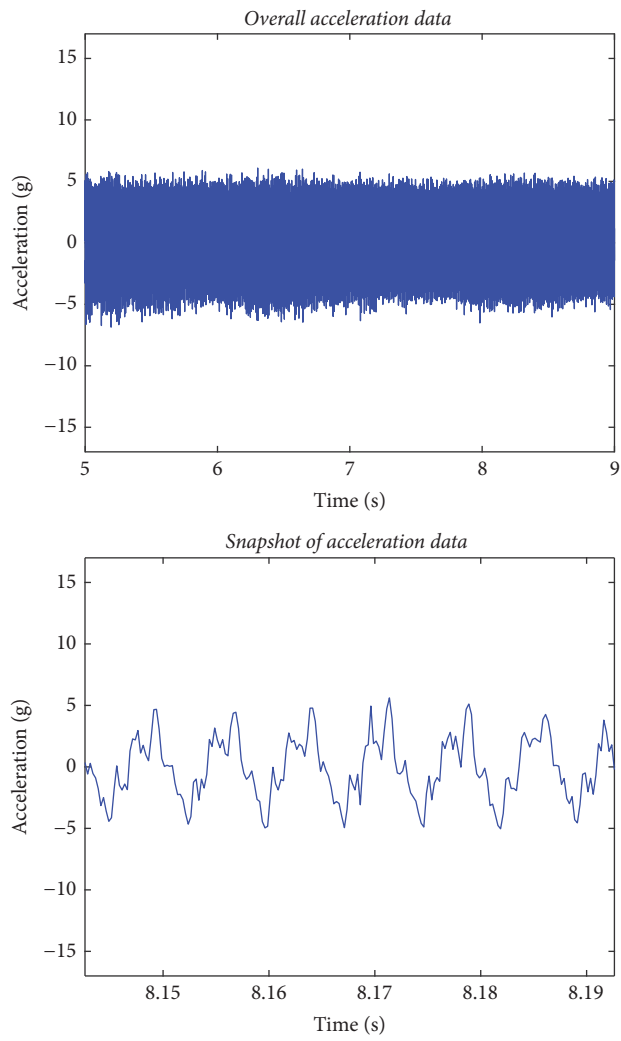


FIGURE 19: Measured acceleration data with wire type shock absorber.

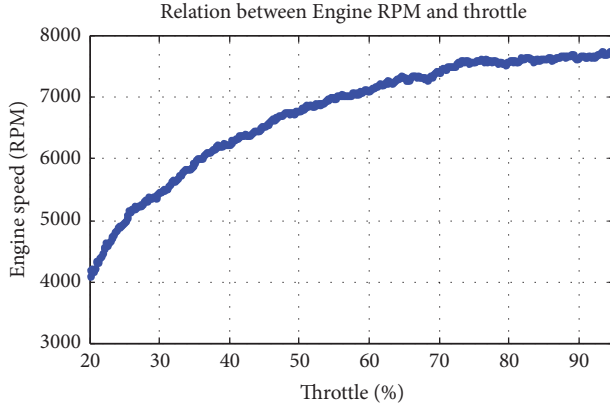


FIGURE 20: Relation between engine RPM and throttle input.

the wire type shock absorbers. This range of vibration can further be handled by both mechanical damper and digital filter of the signal. The shock absorber performance is very favorable in this situation.

3.2. Engine Controller Result. In the QiQ engine controller development and experiment, the gasoline engines are equipped with $16'' \times 10''$ 3-blade propellers from Master Airscrew [[http://www3.towerhobbies.com/cgi-bin/wti0001p?
&I=LXRF51](http://www3.towerhobbies.com/cgi-bin/wti0001p?&I=LXRF51)]. The QiQ uses standard octane 95 gasoline mixed with 3.5% lubrication oil by volume. The ambient condition is 27°C near the sea level. And infrared noncontact thermometer MLX90614 from Melexis [<https://www.melexis.com/en/product/MLX90614/Digital-Plug-Play-Infrared-Thermometer-TO-Can>] is adopted to measure the exhaust pipe temperature of the engine. The sensor has accuracy of $\pm 3^\circ\text{C}$. The point of measurement is located at the exhaust gas outlet from engine. Even though the measured temperature at exhaust nozzle may not represent internal temperature from engine, it is used to indicate the overall temperature of the engine during test.

As discussed earlier, the linearization of the actuator has to be done before the actual PID is implemented. This is done by starting and warming up the engine until its temperature is saturated and stable. After that, the throttle should be slowly increased while monitoring the throttle and engine RPM relation. Since the stability of engine speed under 4000 RPM is poor, the engines may be subjected to cooling down or even shutdown when a sudden change signal is received at very low RPM. The controller design should be working at the region higher than this point.

From Figure 20, it is obvious that the relation between engine speed and throttle input is highly nonlinear. If the PID controller is implemented directly to the throttle, the tuned PID parameters will not be optimized for the whole operation range. The linearization is done by using 3-point spline, where the middle point of data is at 6000 RPM from the throttle. The controller output is scaled first before sending to the servo to form the linearized actuator.

The long-term stability is very important in the proposed QiQ multirotor flight controller system. Even in situation of ambient environmental change, the controller characteristic

and accuracy should remain the same. Temperature is known to be one major factor that affects the engine characteristics. The controller should be able to compensate engine throttle to give the expected power, while the engine has not reached the stable temperature. It also has to reduce compensation fast enough. The open-loop response experiment of the engines is studied to observe engine characteristics and performance without controllers. As engine is started from cool state, it is subjected to immediate throttle input. The reduction of throttle input observes the cooling down effect to the engine power. The response is shown in Figure 21.

At the ignition moment ($t = 0$), engine RPM ramped up sharply, as shown in Figure 21(a). The RPM, however, is hesitated to increase to stable region for few seconds because the engine temperature is not high enough for operating condition. Figure 21(b) shows that the exhaust pipe temperature rises sharply at the beginning. Although exhaust pipe temperature only shows the trend of overall engine temperature, it still indicates the engine condition at that moment. Engine RPM is stable after 15 seconds. This is unacceptable to implement directly into the proposed QiQ system. Large asymmetrical thrust might greatly affect flight stability and performance.

At $t = 90$ s, engine throttle is reduced from 35% to 17%. The RPM drops accordingly. After a period, while engine is cooling down, engine RPM continues to drop from 4100 to 3720 in a minute. This shows the long-term instability of the open-loop system. The compensation mechanism from a feedback controller is required to enable stability for the whole flight.

The RPM control mode of engine controller using the incremental PID has been implemented. The engine starts from cool state at ambient temperature. The RPM setpoint is increased from 4750 RPM to 6700 RPM by pilot controller from the transmitter. After 75 seconds, the setpoint was changed to 4960 RPM and dropped to 4350 RPM after 60 seconds. The controller setpoint is once again raised to 6700 RPM for 60 seconds and then returned to 4350 RPM. The result is as shown in Figure 22.

From Figure 22(a), the engine RPM controller tracks the commanded setpoint accurately even at the sharp edge and instantaneous change. The engine RPM output is controlled and has similar characteristics even if the engine temperature during overall test period has changed by accumulated heat. The effect of controller is clearly seen from Figure 22(b) when controller compensates the throttle to sustain engine RPM at that moment when the engine temperature is not high enough. At $t = 60$ s, the throttle input to engine is 69%, and it is later reduced to 46% after 26 seconds. This throttle compensation can be seen again at $t = 260$ s. It is obvious that the controller compensation is required to allow engine RPM to stay stable at the desired point during transient change of setpoint. The controller performance at steady state can be seen from $t = 290$ s, where the engine RPM has not changed but throttle output has already responded to the small-fluctuated error. At lower RPM from $t = 95$ to $t = 260$ and from $t = 318$ to $t = 400$, the engine temperature drops to make the engine RPM output lower at the same throttle input. But the engine RPM controller slightly compensates it

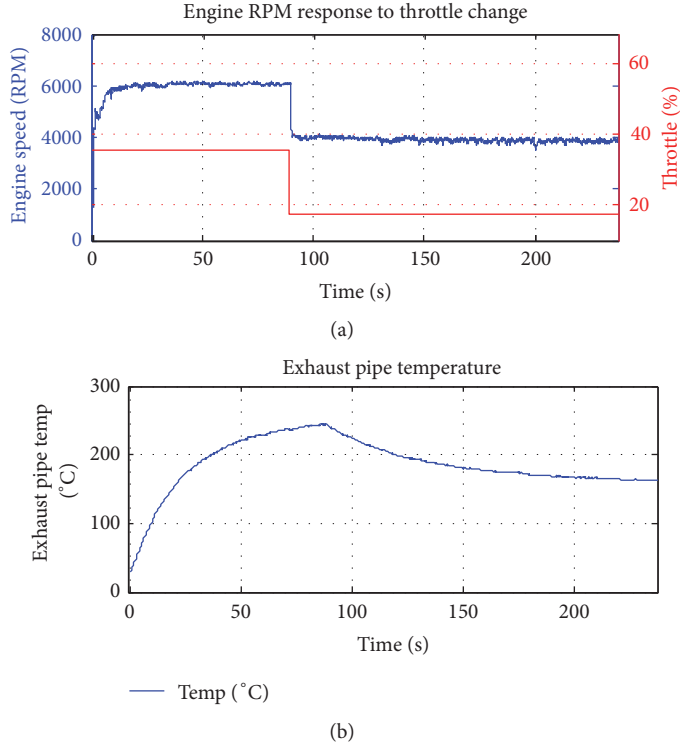


FIGURE 21: (a) Engine RPM response to step input. (b) Corresponding exhaust pipe temperature.

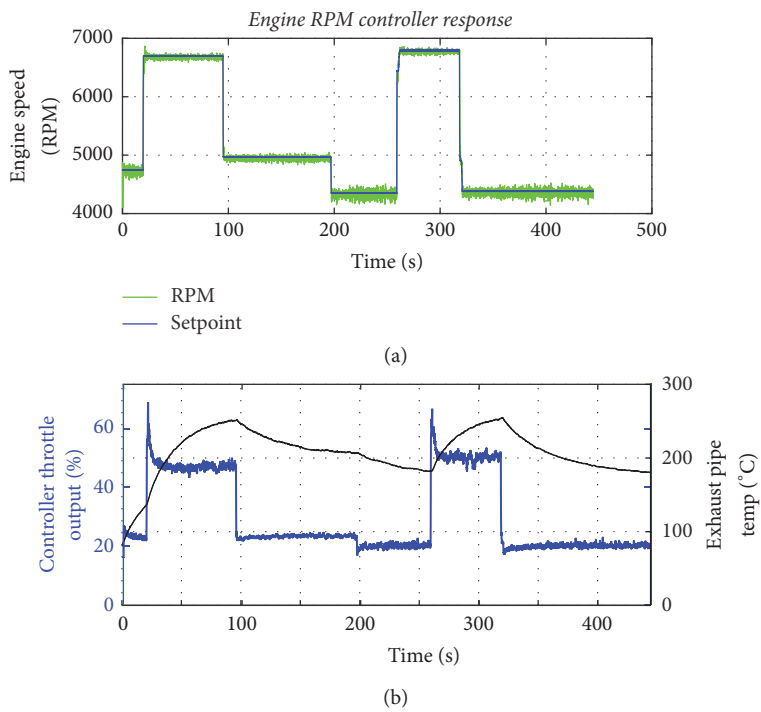


FIGURE 22: (a) Close-loop engine RPM response. (b) Controller throttle output and exhaust temperature.

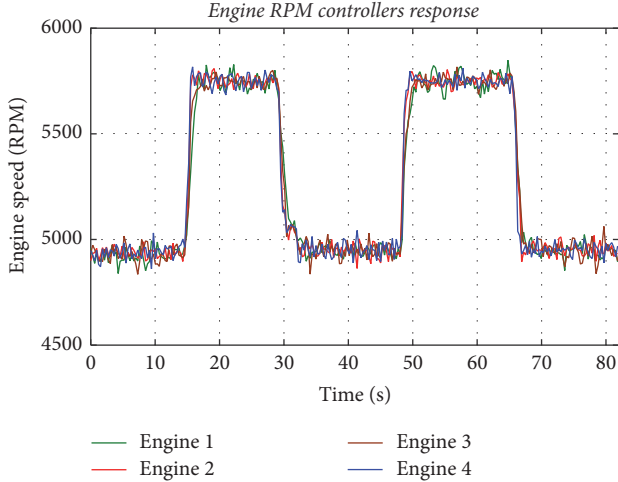


FIGURE 23: Four engines controlled output response.



FIGURE 24: Modified octorotor to simulate QiQ stabilization algorithm.

by increasing throttle slowly according to temperature drop. This proves the effectiveness of the controller in both high and low temperatures.

Another experiment is carried out before flight test. This experiment tests the controller characteristics before flight. It is important to ensure the similarity of the thrust actuator for the proposed QiQ multirotor system. Unbalance thrust may generate excess unwanted moment to destabilize the QiQ. This experiment is completed to ignite all engines and enables RPM controller. After that, step inputs are given to see their responses. The four engines performance is shown in Figure 23.

3.3. Flight Stabilization Simulation. A smaller octorotor system as shown in Figure 24 is set up to simulate and test the characteristics of the flight stabilization. Four motors are located closer to the center to simulate the engines that purely provide thrust without stabilization. The outer four motors are used to stabilize the airframe. The ratio of the radius from motor to the center between inner circle and outer circle is similar to the real design. The inner motor radius is 38 cm and the outer motor radius is 80 cm. A laptop of 14-inch size is used for reference. The total take-off weight is 2.1 kg. The inner quad motors are directly controlled by pilot. They take the same input from radio transmitter directly. The outer quad motors are controlled by flight control system. The pilot

commands pitch angle forward and backward to simulate the step input. Because of limited area, the control cannot be pure step input to avoid dangerous zone, as shown in Figure 25.

From Figure 25(a), the pitch setpoint moves around center to the maximum of ± 30 degrees. The octorotor responds to the setpoint accurately without losing stabilization. Between each pitch up and down, there is small gap to the setpoint. The flight controller is able to stop the fast movement and restore the pitch angle to the desired angle. The similarity in each movement and offset free result is controlled by inner loop of the stabilization. Figure 25(b) shows the stabilizing result of the inner loop rate controller. The rate controller takes input from the angular PD controller. At $t = 1$ when the setpoint is zero and angle is also zero, the output of outer PID is zero too. At $t = 1.4$ when pilot starts to give pitch command, the inner loop setpoint rises sharply to respond to the outer loop command. When the pitch angle reaches setpoint, the inner loop setpoint reduces to zero. This is similar to the situation when the pilot releases control stick to zero. The setpoint of the inner loop goes sharply to pitch the airframe back to level. The response of the airframe is stable and predictable.

Figure 25(c) shows the actual movement of motor throttle command. Motor 1 and motor 2 are placed in the front and back of the airframe, respectively. The offset between two of these motors from 50% throttle shows that either the center of gravity of the aircraft is not in the center or there is external disturbance to the aircraft. These imperfections require the flight control to respond by offsetting the thrust of the motor constantly. It is handled by the integral controller of the inner loop PID. At the point where the fast angular change is required, the difference within motor thrust is enlarged up to the point that it can reach full throttle, while another side drops almost to idle. The QiQ design shows the advantage in this situation where the stabilization motor has maximum authority because it can have the maximum possible thrust between each side of motor from the center. For the heavy lifting quadrotor, the average of the thrust output is nearly at full throttle that very little can be left to stabilize the aircraft.

3.4. Flight Result of the QiQ Prototype. Flight test on this dual powered multirotor system with the proposed QiQ configuration has been successfully completed. The flight test was conducted in the morning of clear day. Ambient temperature was 27°C , with no sign of rain, and the wind was calm. The control strategy gives all engines to run at the same RPM. Since the engines are started at 10% throttle, the outer electric DC brushless motors are set at 60% throttle to maximize their possible control range. The engine RPM is continuously increased until take-off. The flight was stable. The aircraft was fully controlled by pilot. Its characteristic is similar to the conventional multirotor systems. However, the control in yaw direction has been slightly delayed due to high inertia in the axis. The test flight data are shown in Figure 26.

The control range was reduced because of flying area limitation and for safety of the experiment. The flight controller has ability to stabilize the QiQ airframe in every movement. Even though the movement is small, the precision in control has been demonstrated in Figure 26 that the actual pitch

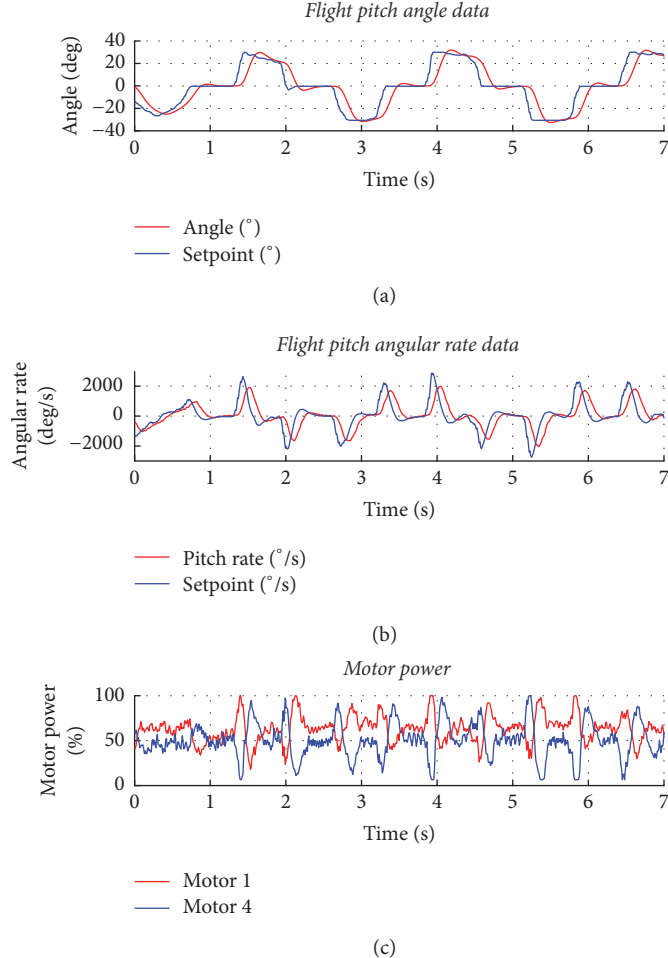


FIGURE 25: Experiment flight data of simulated octocopter.

angle follows the setpoint data accurately. The QiQ system stability was observed with no overshoot or control failure. From Figure 26(b), the gyroscope was disturbed slightly from the vibration of the engine. The noise level is higher than the simulator airframe, but the signal-to-noise ratio is high enough to overcome the control effort. The motor output on Figure 26(c) shows the effect of vibration to sensor signal which affects motor output. Because of the error caused from the gyroscope noise, the motor output resulted from this error and PID gain. The result confirms that the shock absorber is necessary and effective in order to prevent losing stabilization caused by engine vibrations.

Engine controller is able to hold the engine at desired throttle throughout the flight. The variation in engine RPM is about ± 100 RPM which is considered relatively small, that is, $100/5800 < 2\%$, where the electrical motor stabilization can handle this error and prevent destabilization of system. Engine RPM data output rate is only 4 Hz transferred through CAN Bus, while other data are recorded at 100 Hz. This is why the RPM data appears to have slightly different smoothness compared to the other data. The deviation in engine RPM is also another reason that causes the noisy motor data because the motors need to respond to the disturbance created by

those unexpected imbalances lifting force from engine RPM deviation. The proposed QiQ in 16 kg payload test is shown in Figure 27. The payload is bricks beneath the center disc.

After preliminary flight verifications, the proposed QiQ is added with a composite fuel tank for better performance. The fuel tank is made of glass fiber and is fabricated as shown in Figure 28. The inner tank contains four separation walls to avoid fuel splash inside the tank and a tilt inside bottom to guide the fuel flow out. The space beneath the fuel tank bottom can be used for batteries or electronics. The fuel tank has a top cover to accept the GPS antenna with signal wires to go through to the bottom. The weight of fuel tank is 2.1 kg with capacity of 14 liters. The full assembly of the QiQ multirotor system is as shown in Figure 30.

The purpose of the heavy lift multirotor is usually related to high inertia airframe configuration. There are some specific applications that require intensive heading control, for example, agricultural drone, where the spray array needs to be perpendicular to the flight path. The heading control for conventional multirotor relies on difference of propeller generated torque between clockwise and counterclockwise rotating direction of the motor as can be seen from Figure 4. However, as the size increases, the inertia also increases. The

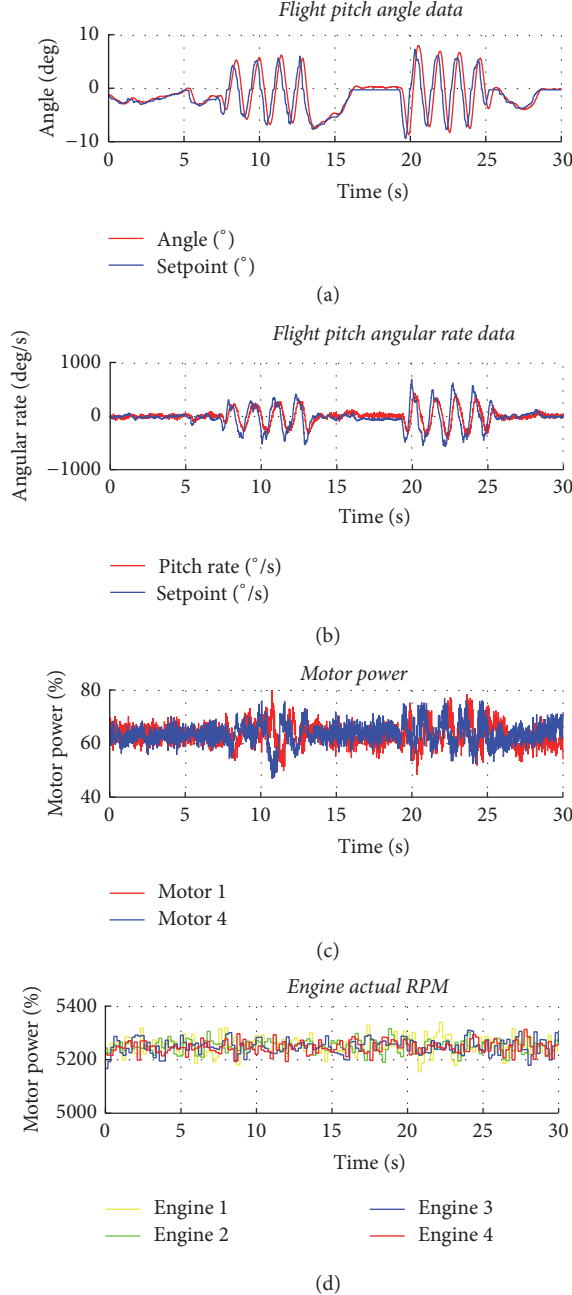


FIGURE 26: Experiment flight data of QiQ prototype.

moment of inertia of a point mass is square proportional to the distance of the mass to center of gravity. But as the frame size increases, the torque generated by propeller does not increase in the same scale. To improve the flight controllability in the later experiment, a small attitude fin is added under the motor, as shown in Figure 24, to deflect down flow by controlled moment.

In the top of Figure 29, the fin constructed from Styrofoam is installed right under the propeller downstream of electric airframe. Each of the flaps is driven by servo motor to control the angle of deflection. The figure below shows the propeller air stream passing through the fin at different situation. The fin acts as airfoil with flap deflection generating

the lateral forces. In this stage, the deflection of each fin is on the same side that produces the torque to generate moment in the same side. By adding the effect of lateral fin to moment equation (see (11c)), the equation becomes

$$M_z = M_a - M_b + M_c - M_d - M_1 + M_2 - M_3 + M_4 + f_1 l_1 + f_2 l_2 + f_3 l_3 + f_4 l_4. \quad (16)$$

This modification adds the direct control to the directional control of multirotor. The control authority also increases with size and reduces the required motor rotation speed change to control the attitude which expands flight



FIGURE 27: The proposed QiQ prototype in 16 kg flight test.

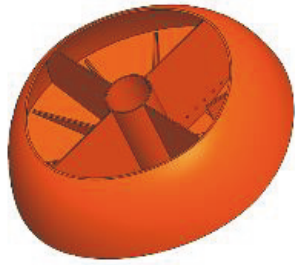


FIGURE 28: Composite fuel tank sectional view.

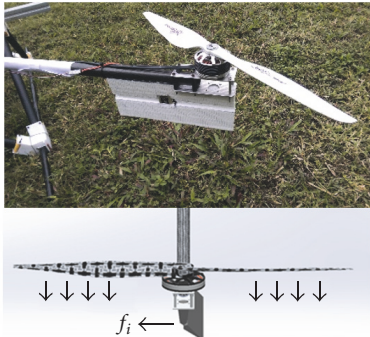


FIGURE 29: Attitude control fin.



FIGURE 30: QiQ with composite fuel tank and attitude control fins.

envelope. The idea is suitable not only for QiQ but also for other large multirotors.

4. Conclusion

The idea of gasoline-electric dual power multirotor vertical take-off/landing vehicle is designed, fabricated, implemented, and proven to be feasible and valuable for more practical developments. Gasoline engines are able to provide major lift, while BLDC motor has better performance in system stabilization. The engine RPM controller can stabilize and normalize the engine characteristics into safe margin. Flight stabilization controller is also able to provide real-time response even in extreme case as in simulated airframe or precise control in real prototype flight test. The proposed QiQ design can be optimized and improved into further applications.

Conflicts of Interest

The authors declare that they have no conflicts of interest.

Acknowledgments

This work is supported by Ministry of Science and Technology (MOST) under Research Project MOST-105-2119-M-006-012.

References

- [1] A. A. Mian and D. Wang, "Nonlinear flight control strategy for an underactuated quadrotor aerial robot," in *Proceedings of 2008 IEEE International Conference on Networking, Sensing and Control, (ICNSC '08)*, pp. 938–942, Sanya, China, April 2008.
- [2] B. Scrosati and J. Garche, "Lithium batteries: status, prospects and future," *Journal of Power Sources*, vol. 195, no. 9, pp. 2419–2430, 2010.
- [3] H. Chen, T. N. Cong, W. Yang, C. Tan, Y. Li, and Y. Ding, "Progress in electrical energy storage system: a critical review," *Progress in Natural Science*, vol. 19, no. 3, pp. 291–312, 2009.
- [4] M. Muhammad, N. H. Hamid, A. F. Malik, N. B. Z. Ali, and M. T. Jan, "A review on key issues and challenges in devices level mems testing," *Journal of Sensors*, vol. 2016, Article ID 1639805, 2016.
- [5] S. Kon, K. Oldham, and R. Horowitz, "Piezoresistive and piezoelectric MEMS strain sensors for vibration detection," in *Proceedings of sensors and smart structures technologies for civil, mechanical, and aerospace systems 2007*, San Diego, California, March 2007.
- [6] H. L. Chang, L. Xue, W. Qin, G. M. Yuan, and W. Z. Yuan, "An integrated MEMS gyroscope array with higher accuracy output," *Sensors*, vol. 8, no. 4, pp. 2886–2899, 2008.
- [7] N. Tadrist, H. Zeroug, and B. Boukais, "Development of brushless d.c. motor drive system for teaching purposes using various PWM control techniques," *International Journal of Electrical Engineering Education*, vol. 49, no. 3, pp. 210–231, 2012.
- [8] J. Shi and T.-C. Li, "New method to eliminate commutation torque ripple of brushless DC motor with minimum commutation time," *IEEE Transactions on Industrial Electronics*, vol. 60, no. 6, pp. 2139–2146, 2013.

- [9] B. J. Varocky, "Benchmarking of Regenerative Braking for a Fully Electric Car," Eindhoven University of Technology, 2011.
- [10] H. M. Huang, G. M. Hoffmann, S. L. Waslander, and C. J. Tomlin, "Aerodynamics and control of autonomous quadrotor helicopters in aggressive maneuvering," in *Proceedings of the IEEE International Conference on Robotics and Automation (ICRA '09)*, pp. 3277–3282, IEEE, Kobe, Japan, May 2009.
- [11] S. Driessens and P. E. I. Pounds, "Towards a more efficient quadrotor configuration," in *Proceedings of 26th IEEE/RSJ International Conference on Intelligent Robots and Systems: New Horizon, (IROS '13)*, pp. 1386–1392, Tokyo, Japan, November 2013.
- [12] J. Macheret, J. Teichman, and R. Kraig, "Conceptual Design of Low-Signature High- Endurance Hybrid-Electric UAV," *IDA., Virginia, IDA Doc*, 2011.
- [13] eCalc-Online propeller calculator <http://www.ecalc.ch>.
- [14] R. Godzankier, M. J. Rutherford, and K. P. Valavanis, "Improving endurance of autonomous aerial vehicles through intelligent service-station placement," in *Proceedings of the IEEE International Conference on Robotics and Automation*, pp. 3179–3184, Saint Paul, MN, USA, May 2012.
- [15] J. Lieh, E. Spahr, A. Behbahani, and J. Hoying, "Design of hybrid propulsion systems for unmanned aerial vehicles," in *proceeding of AIAA/ASME/SAE/ASEE Joint Propulsion Conference & Exhibit*, San Diego, CA, USA, Aug 2011.
- [16] IOR Energy, "List of common conversion factors (engineering conversion factors)," <https://web.archive.org/web/20100825042-309/>, <http://www.ior.com.au/ecflist>.
- [17] M. M. Thackeray, C. Wolverton, and E. D. Isaacs, "Electrical energy storage for transportationapproaching the limits of, and going beyond, lithium-ion batteries," *Energy Environmental Science*, vol. 5, pp. 7854–7863, 2012.
- [18] K. K. Bhamidipati, D. Uhlig, and N. Neogi, "Safety and reliability into uav systems: mitigating the ground impact hazard," in *proceeding of the Navigation and Control Conference and Exhibit*, August 2007.
- [19] C. E. Lin, T. Supsukbaworn, Y.-C. Huang, and K.-T. Jhuang, "Engine controller for hybrid powered dual quad-rotor system," in *Proceedings of 41st Annual Conference of the IEEE Industrial Electronics Society, (ECON '15)*, pp. 1513–1517, Yokohama, Japan, November 2015.
- [20] T. Luukkonen, *Modelling and control of quadcopter [Master, thesis]*, Aalto University, 2011.
- [21] Bosch., *Automotive Handbook*, vol. 5th, Bosch Gmbh, 2000.
- [22] L.-B. Fredriksson, "CAN for critical embedded automotive networks," *IEEE Micro*, vol. 22, no. 4, pp. 28–35, 2002.

